Atmospheric
Chemistry
and Physics
Discussions

1 **Speciated Atmospheric Mercury during Haze and Non-haze Days in**

2 **an Inland City in China**

3

4

5 Qianqian Hong[1,3], Zhouqing Xie[1,2,3*], Cheng Liu[1,2,3*], Feiyue Wang[4], Pinhua Xie[2,3],

6 Hui Kang[1], Jin Xu[2], Jiancheng Wang[1], Fengcheng Wu[2], Pengzhen He[1], Fusheng Mou[2],

7 Shidong Fan[1], Yunsheng Dong[2], Haicong Zhan[1], Xiawei Yu[1], Xiyuan Chi[1], Jianguo

8 Liu[2]

9

10

11 1. School of Earth and Space Sciences, University of Science and Technology of

12 China, Hefei, 230026, China

13 2. Innovation Center for Excellence in Urban Atmospheric Environment of CAS &

14 Institute of Urban Environment of CAS, Xiamen, 361021, China

15 3. Key Lab of Environmental Optics & Technology, Anhui Institute of Optics and

16 Fine Mechanics, Chinese Academy of Sciences, Hefei, 230031, China

17 4. Department of Environment and Geography, University of Manitoba, Winnipeg,

18 Canada

19

20

21 Correspondence author:

22 zqxie@ustc.edu.cn (Z.Q.X.); chliu81@ustc.edu.cn (C.L.)

23

24

Atmospheric
Chemistry
and Physics

Open Access

EGU

Discussions

25 **Abstract.** Long-term continuous measurements of speciated atmospheric mercury

26 were conducted at Hefei, a mid-latitude inland city in east central China, from July

27 2013 to June 2014. The mean concentrations ($\pm$ standard deviation) of gaseous

28 elemental mercury (GEM), reactive gaseous mercury (RGM) and particle-bound

29 mercury (PBM) were 3.95 $\pm$ 1.93 ng m^{-3}, 2.49 $\pm$ 2.41 pg m^{-3} and 23.3 $\pm$ 90.8 pg m^{-3},

30 respectively, during non-haze days, and 4.74 $\pm$1.62 ng m^{-3}, 4.32 $\pm$ 8.36 pg m^{-3} and

31 60.2 $\pm$ 131.4 pg m^{-3}, respectively, during haze days. Potential source contribution

32 function (PSCF) analysis suggested that the atmospheric mercury pollution during

33 haze days was caused primarily by local mercury emissions, instead of via long-range

34 mercury transport. In addition, the disadvantageous diffusion during haze days will

35 also enhance the level of atmospheric mercury. Compared to the GEM and RGM,

36 change in PBM was more sensitive to the haze pollution. The mean PBM

37 concentration during haze days was 2.5 times that during non-haze days due to

38 elevated concentrations of particulate matter. A remarkable seasonal trend in PBM

39 was observed with concentration decreasing in the following order in response to the

40 frequency of haze days: autumn, winter, spring, summer. A distinct diurnal

41 relationship was found between GEM and RGM during haze days, with the peak

42 values of RGM coinciding with the decline in GEM. Using HgOH as an intermediate

43 product during GEM oxidation, our results suggest that NO_2 aggregation with HgOH

44 could explain the enhanced production of RGM during the daytime in haze days.

45 Increasing level of NOx will potentially accelerate the oxidation of GEM despite the

46 decrease of solar radiation.

47

48

Atmospheric
Chemistry
and Physics
Discussions

1. Introduction

49

50   Mercury (Hg) is an environmental pollutant that has received much global

51   attention because of its toxicity and bioaccumulation via the aquatic food chain. The

52   most important transport pathway of mercury is via the atmosphere (Schroeder and

53   Munthe, 1998;Lindqvist and Rodhe, 1985). Operationally, atmospheric mercury is

54   commonly differentiated into three forms: gaseous elemental mercury (GEM),

55   reactive gaseous mercury (RGM) and particle-bound mercury (PBM). The sum of

56   these three atmospheric speciated mercury is defined as total atmospheric mercury

57   (TAM = GEM + RGM + PBM), and the sum of GEM and RGM is known as total

58   gaseous mercury (TGM = GEM + RGM) (Gustin and Jaffe, 2010;Gustin et al., 2015).

59   GEM is regarded as the predominant form of atmospheric mercury, accounting for

60   over 95% of the total. GEM is stable in the atmosphere with a long residence time

61   (0.5–2 yr) and can be transported at the regional to global scale (Schroeder and

62   Munthe, 1998;Lindberg et al., 2007). GEM can be oxidized to RGM through

63   photochemical processes, and further transformed to PBM on aerosol surfaces.

64   Although GEM is the predominant form of mercury in the air, trace amounts of RGM

65   and PBM control the mercury scavenged from the atmosphere (Lindberg and Stratton,

66   1998). RGM and PBM can be readily removed form the air by wet and dry deposition

67   as a result of their high surface reactivity and water solubility (Lindqvist and Rodhe,

68   1985). Thus, the chemical transformations between GEM, RGM and PBM will

69   directly influence the atmospheric lifetime of mercury.

70   As a result of the rapid industrial development and economic growth of recent

71   decades, China has become one of the major contributors to anthropogenic mercury

72   emissions to the environment (Wu et al., 2006;Pacyna et al., 2006;Streets et al., 2005).

Atmospheric
Chemistry
and Physics
Discussions

73   Atmospheric mercury emissions from anthropogenic sources in China have been

74   estimated to be in the range of 500-700 tons/yr, accounting for 25-30% of the total

75   global anthropogenic mercury emissions (Streets et al., 2005;Wu et al., 2006).

76   Research into atmospheric mercury in China is therefore critical to the understanding

77   of mercury cycling at both regional and global scales. Long-term observation of

78   atmospheric mercury has been conducted in different regions in China, including both

79   urban and remote areas. TGM concentrations observed in urban and industrial regions

80   of China were in the range of 2.7–35 ng m^{-3}, higher than the values reported for North

81   America and Europe, and for the adjacent Asian countries such as Korea and Japan

82   (Stamenkovic et al., 2007;Dommergue et al., 2002;Fang et al., 2009). TGM and PBM

83   concentrations in remote areas of China were also found to be higher than those

84   observed in North America and Europe (Fu et al., 2008a;Fu et al., 2008b;Fu et al.,

85   2012;Liu et al., 2010).

86   In recent years, haze pollution has become a major concern in China due to its

87   impacts on visibility, air quality, and climate. It is well known that haze formation is

88   mainly dependent on the atmospheric relative humidity (RH) and the concentration of

89   airborne particles (Chen et al., 2003;Sun et al., 2013). Most studies on haze have

90   focused on the measurements of airborne particulate matter; few examined the

91   influence of haze on the chemistry of atmospheric mercury, especially PBM. In this

92   study, we conducted one year synchronous observations of speciated atmospheric

93   mercury in Hefei, an inland city of China, which experiences frequent haze events.

94   The comparision of atmospheric mercury under haze days and non-haze days during

95   the study period allows us to examine the formation and deposition mechanisms of

96   mercury, as well as their temporal variations.

Atmospheric
Chemistry
and Physics
Discussions

Open Access

EGU

2.   Methods

2.1 Study site

99   Continuous measurements of speciated atmospheric mercury were undertaken in

100   Hefei (31 °52′ N, 117°17′ E) from July 2013 to June 2014. Hefei, the capital of Anhui

101   Province, is located in east central China, between the Changjiang (Yangtze River) and

102   the Huaihe (Huai River). Hefei has a humid subtropical climate with four distinct

103   seasons: June-August is considered summer, September-November autumn,

104   December-February winter and March-May spring. The prevailing wind is

105   southeasterly in summer and northwesterly in winter. Like many Chinese cities, Hefei

106   has experienced rapid growth in the past 20 years. The total permanent population is

107   about 7.7 million.

108   The monitoring site was located on the Science Island, a small peninsula on the

109   Dongpu Reservoir in the northwestern outskirts of Hefei (Fig. 1). The sampling and

110   analytical instruments were installed 1.5 m above the rooftop (~ 20 m above the

111   ground) of the main building of Anhui Institute of Optics and Fine Mechanics. Further

112   information about the monitoring site can be found in a previous study (Hu et al.,

113   2014). We chose this area as the monitoring site because it is one of the cleanest areas

114   in Hefei, not adjacent to any direct pollution sources such as power plants, iron and

115   steel works.

116

2.2 Measurements of speciated atmospheric mercury

118   From July 2013 to June 2014, simultaneous measurements of speciated

119   atmospheric mercury concentrations were performed by an automated Tekran[TM]

120   mercury speciation system. The system consisted of a Model 2537B mercury analyzer

Atmospheric
Chemistry
and Physics
Discussions

Open Access

EGU

121   combined with a Model 1130 RGM unit and a Model 1135 PBM unit. The system was

122   configured to measure GEM every 5 min., and RGM and PBM every 2 two hr.

123   The details about the Tekran-based mercury speciation system can be found in

124   Landis et al. (2002). In general, the automated measurement process can be

125   summarized as sample collection, thermal desorption and determination. During the

126   collection period, ambient air was drawn to the system at a flow rate of 10 L/min.

127   RGM and PBM in the air were captured by a KCl-coated quartz annular denuder in

128   the 1130 unit and a quartz filter in the 1135 unit, respectively, whereas GEM would

129   pass through the denuder and filter and be quantified on the Tekran 2537B by

130   cold-vapor atomic fluorescence spectroscopy (CVAFS). After an hour of sampling, the

131   1135 quartz filter and the 1130 denuder would be switched to the thermal

132   decomposition mode at 800 ℃ and 500 ℃, respectively, with the resulting Hg^0

133   quantified by the 2537B unit in the next hour, while the 1135 and 1130 components

134   were flushed with zero-mercury gas for the next sampling.

135   The instrument maintenance followed typical protocols used in similar studies

136   (Landis et al., 2002;Hu et al., 2014). The quartz annular denuder was recoated every

137   two weeks, the quartz filter was replaced once a month, and the Teflon filter (pore size

138   0.2 μm) in the sample inlet was changed every two weeks. Automated recalibration of

139   the Tekran 2537B was performed every 25 h using an internal mercury permeation

140   source. No calibration standards were available for RGM and PBM, but the 1σ

141   precision for RGM and PBM was about 15 % (Landis et al., 2002). The detection

142   limit in ambient air is about 0.5 ng m^{-3} for GEM (or TGM) at a resolution of 5 min,

143   and 1 pg m^{-3} for RGM and PBM at a resolution of 2 h (Gustin et al., 2015). Although

144   the Tekran-based mercury speciation technique has been widely used around the

Atmospheric
Chemistry
and Physics
Discussions

Open Access

EGU

145   world, recent studies have shown that the technique does not efficiently collect all

146   gaseous oxidized mercury and thus may substantially underestimate the concentration

147   of reactive mercury (Huang et al., 2013;Gustin et al., 2013). Therefore, the RGM

148   values reported in this study should be considered as the lower limits of gaseous

149   oxidized mercury in the air (Wang et al., 2014).

150

151   **2.3 Ancillary Data**

152   Standard meteorological measurements including air temperature, air pressure,

153   RH, wind direction and speed were observed with a 5-min resolution. CO was

154   measured by an automated infrared carbon monoxide analyzer (Model EC9830T,

155   Ecotech Inc., Australia), with a detction limit of 40 ppbv. O_3 was measured every 5

156   min by an ozone analyzer (Model EC9810B, Ecotech Inc., Australia); its detection

157   limit and accuracy are 0.5 ppbv and 0.001 ppm, respectively. NO_2 was measured by a

158   Multi axis differential optical absorption spectroscopy (MAX-DOAS) instrument. The

159   collected spectra were analyzed using the QDOAS spectral fitting software suite

160   developed at BIRA-IASB (http://uv-vis.aeronomie.be/software/QDOAS/). We used

161   the geometric approximation for conversion between slant column densities (SCDs)

162   and vertical column densities (VCDs) (Ma et al., 2013). $PM_{2.5}$ (particulate matter less

163   than 2.5 μm in diameter) data are collected from China air quality online analysis

164   platform (http://www.aqistudy.cn/historydata/index.php). In addition, 24-hr PM_{10}

165   (particulate matter less than 10 μm in diameter) samples were collected on glass-fiber

166   filters by a high-volume sampler during heavy pollution episodes (from 10 Nov to 9

167   Dec 2013, n=11). Water-soluble ions in the PM_{10} samples were determined by ion

168   chromatography (Model ICS-2100, Dionex). In order to identify the potential source

Atmospheric
Chemistry
and Physics
Discussions

169   of mercury, NASA's satellite hotspots/fire locations information were obtained from

170   the   Fire   Information   for   Resource   Management   System   (FIRMS)

171   (https://firms.modaps.eosdis.nasa.gov/firemap/).

172

173   **2.4 Potential Sources Contribution Function (PSCF) analysis**

174   To identify the possible influence of long-range transport on the distribution of

175   atmospheric mercury in Hefei, we calculated backward trajectories of air masses

176   using the HYSPLIT (Hybrid Single-particle Lagrangian Integrated Trajectory) model

177   with the Global Data Assimilation System (GDAS 1°) developed by the National

178   Oceanic and Atmospheric Administration (NOAA) (*http://www.ready.noaa.gov*)

179   (Draxler and Hess, 1998). Considering the atmospheric pollutants are mainly

180   concentrated in the low altitude during heavy pollution days, the trajectory arrival

181   heights were set at 500 m to represent the boundary layer where atmospheric

182   pollutants were well mixed. In this study, 5-day back-trajectories were calculated in

183   ensemble forms which calculate 27 trajectories from the selected starting point (31°52′

184   N, 117°17′ E) (Fain et al., 2009).

185   The contributions of other pollution source regions to the atmospheric mercury at

186   Hefei was identified by the Potential Sources Contribution Function (PSCF) analysis

187   with the TrajStat software (Wang et al., 2009). PSCF analysis has been shown to be

188   useful in spatially identifying pollution sources for pollutants with a long lifetime

189   such as elemental mercury and CO (Xu and Akhtar, 2010). The PSCF values for the

190   grid cells in the study domain were calculated by counting the trajectory segment

191   endpoints that terminate within each cell. The number of endpoints that fall in the ij_{th}

192   cell is designated as N_{ij}. The number of endpoints for the same cell corresponding to

Atmospheric
Chemistry
and Physics

Discussions

Open Access

193   the atmospheric mercury concentration higher than an arbitrarily set criterion (4 ng

194   m^{-3} which was the mean GEM concentration during the whole study period) is

195   defined to be M_{ij}. The PSCF value for the ij_{th} cell is then defined as:

196    $$\text{PSCF}_{ij} = \frac{M_{ij}}{N_{ij}} W_{ij}$$ (2)

197   W_{ij} is an arbitrary weight function to reduce the effect of small values of N_{ij}. The

198   PSCF values were multiplied by W_{ij} to better reflect the uncertainty in the values for

199   these cells (Polissar et al., 2001). The weight function reduces the PSCF values when

200   the total number of endpoints in a particular cell is less than 3 times the average value

201   of the end points per cell:

202    $$W_{ij} = \begin{cases} 1.0 & N_{ij} \geq 3N_{ave} \\ 0.70 & 3N_{ave} > N_{ij} \geq 1.5N_{ave} \\ 0.40 & 1.5N_{ave} > N_{ij} \geq N_{ave} \\ 0.20 & N_{ave} > N_{ij} \end{cases}$$ (3)

203

204   **3. Results**

205   We intended to continuously monitor speciated atmospheric mercury

206   concentration over the course of a year; however, interruptions were inevitable due to

207   instrument maintenance, which resulted in loss of data for the following four periods:

208   (1) 25 September to 9 October 2013; (2) 5-14 November 2013; (3) 9-25 February

209   2014; and (4) 1-14 April 2014. The rest of the data were grouped into haze days and

210   non-haze days according to the China Meteorological Administration's haze standard

211   (QX/T 113-2010). Haze days refer to the days when the atmospheric visibility < 10

212   km and RH < 80% (Duan et al., 2016), and non-haze days refer to clear days with the

213   atmospheric visibility > 10 km. The visibility and RH information were collected

214   from   the   weather   history   data   at   the   Luogang   Airport   of   Hefei

Atmospheric
Chemistry
and Physics
Discussions

215   (http://www.wunderground.com/). Through the study period of almost a year, a total

216   of 56 days were identified to be haze days, and 253 days to be non-haze days. All the

217   times reported herein are local time (UTC + 8 hr).

218

219   **3.1   Overall characteristics of speciated atmospheric mercury**

220   The time series of GEM, RGM and PBM concentrations at the study site

221   throughout the study period are shown in Fig. 2, and their frequency distributions are

222   shown in Fig. S1 (in the supporting information). The mean ($\pm$ standard deviation)

223   GEM, RGM and PBM concentrations during the whole study period were 4.07 ± 1.91

224   ng m^{-3}, 3.67 ± 5.11 pg m^{-3}, and 30.0 ± 100.3 pg m^{-3}, respectively (Table 1). The GEM

225   concentrations in different seasons did not differ much. The highest GEM

226   concentration occurred in autumn (4.51 ± 2.10 ng m^{-3}), while the lowest in spring

227   (3.89 ± 1.79 ng m^{-3}). RGM concentrations varied greatly during the study period with

228   much higher concentrations in autumn and the lowest in winter. A similar seasonal

229   variation in the RGM concentration was observed at a remote site in Mt. Gongga of

230   southwest China (Fu et al., 2008b). The seasonal trend in PBM was also observed in

231   Hefei with its concentration decreasing in the following order: autumn > winter >

232   spring > summer. The mean PBM concentration during the cold season was about 20

233   times that in summer, similar to the findings from many previous studies in China

234   (Zhang et al., 2013;Fu et al., 2011;Fu et al., 2008b;Fang et al., 2001).

235   Comparisons of speciated atmospheric mercury concentrations with other urban

236   and rural areas in China and a few other countries are shown in Table 2. The mean

237   GEM concentration at Hefei is slightly higher than that in many remote areas in China

238   (Fu et al., 2008a;Fu et al., 2008b;Fu et al., 2012;Wan et al., 2009a;Wan et al.,

Atmospheric
Chemistry
and Physics
Discussions

Open Access

EGU

239   2009b;Zhang et al., 2015a), but is much lower than those in urban areas of industrial

240   cities such as Guiyang and Changchun where large point sources of mercury exist

241   (e.g., non-ferrous metal smelting, coal-fired power plants, and residential coal burning)

242   (Feng et al., 2004;Fu et al., 2011;Fang et al., 2004). Although Hefei is geographically

243   close to Shanghai, a mega urban centre in China, it is interesting to note that the TGM

244   concentration of Shanghai is much lower than that of Hefei. This may be due to the

245   fact that Shanghai is a coastal city that is influenced more by cleaner marine air

246   masses (Friedli et al., 2011). Table 2 also shows that the average concentration of

247   GEM in Hefei is typically more than two folds that in the urban and rural areas in

248   Europe and North America.

249

250   **3.2   Speciated atmospheric mercury during non-haze days**

251   The frequency distribution of GEM, RGM and PBM for the non-haze period are

252   shown in Fig. S1 (in blue). The mean concentration of GEM was 3.95 $\pm$ 1.93 ng m^{-3}.

253   Its distribution was characterized by large fluctuations ranging from 0.2 to 23.8 ng

254   m^{-3}, although more than half of the GEM values were in the narrow range 2-4 ng m^{-3}.

255   The mean concentration of RGM was 2.49 $\pm$ 2.41 pg m^{-3} with a range of 0.5-33.5 pg

256   m^{-3}, although most of the values were in the range of 1-4 pg m^{-3}. High concentrations

257   of RGM (exceeding 10 pg m^{-3}) only accounted for 1.4% of the total data. The mean

258   RGM concentration at the Hefei site is much smaller than that reported from other

259   study sites in China (Table 2), but is comparable to the values observed from many

260   European and North American sites (Brooks et al., 2010;Li et al., 2008;Liu et al.,

261   2010;Cheng et al., 2014). The mean PBM concentraion at the Hefei site during the

262   non-haze days was 23.3 $\pm$ 90.8 pg m^{-3} with an exceptionally large range of 0.5-1827

Atmospheric
Chemistry
and Physics
Discussions

263   pg m^{-3}. The frequency distribution of PBM showed that high PBM concentrations

264   (i.e., > 50 pg m^{-3}) accounted for 6.4% of the total data. The PBM concentration under

265   the non-haze condition in Hefei is generally at a similar level to the remote areas, such

266   as Mt. Gongga, Mt. Waliguan and Shangri-Li in western China.

267   Diurnal variations of GEM, PBM and RGM concentrations for non-haze days are

268   shown in Fig. 3. Both GEM and PBM concentrations exhibited similar variations with

269   elevated concentrations during night. The RGM concentration during the daytime was

270   slightly higher than that in nighttime, typically peaking between 10:00 and 12:00.

271

272   **3.3   Speciated atmospheric mercury during haze days**

273   Haze pollution mainly occurred in December and January at our monitoring site.

274   The four major haze pollution periods were identified in grey in Fig. 2. The mean

275   concentrations of GEM, RGM and PBM during these haze days were 4.74 $\pm$ 1.62 ng

276   m^{-3}, 4.32 $\pm$ 8.36 pg m^{-3} and 60.2 $\pm$ 131.4 pg m^{-3}, respectively (Table 1). The frequency

277   distributions of GEM, RGM and PBM for the haze days are shown in Fig. S1 (in

278   gray). Comparison of GEM, RGM and PBM concentrations during haze and non-haze

279   days is shown in Fig. 4. GEM, RGM and PBM concentrations show siginificant

280   differences between haze and non haze days (p<0.001, t-test). On average, the

281   concentration of GEM in haze days was 1.2 times that in non-haze days. Similarly, the

282   concentration of RGM in haze days was about 1-1.7 times those in non-haze days.

283   The largest impact of haze pollution is however on PBM, with the mean PBM

284   concentration in haze days about 2.5 times that of non-haze days. High concentrations

285   of RGM (exceeding 10 pg m^{-3}) and PBM concentrations (exceeding 50 pg m^{-3}) were

Atmospheric
Chemistry
and Physics
Discussions

Open Access

286   also more frequently observed than in non-haze days, accounting for 5.9% and 25%,

287   respectively, of the total haze days.

288   Diurnal variations of GEM, PBM and RGM concentrations for haze days are

289   shown in Fig. 3. GEM concentrations were higher during night, decreased during

290   daytime. The opposite pattern was observed for RGM, which showed higher

291   concentrations during daytime than during night; the duration of the RGM peak also

292   lasted longer for haze days. On the contrary, the PBM typically peaked just before

293   sunrise, with the lowest values occurred in the afternoon (14:00-16:00).

294

295   **4.   Discussion**

296   **4.1 Influence of atmospheric mercury emission source**

297   The statistically significant difference in the GEM concentration between

298   non-haze days and haze days suggests that haze pollution could directly affect the

299   concentration of elemental mercury. In order to understand the mercury sources

300   attribution during haze days, the PSCF model analysis was conducted by using the

301   TrajStat software. As shown in Fig. 5, the area south to the monitoring site and the

302   neighboring provinces were the main sources region during haze days. Thus,

303   atmospheric mercury in haze days were mainly affected by local or regional emission

304   sources.

305   The seasonal sources could also be inferred from the PSCF analysis with the

306   year-round data. Fig. 6(A) showed the overall spatial contribution of mercury

307   emission sources in China. As Hefei is located in east-central China, its atmospheric

308   mercury concentration could be affected by both north and south emission sources,

309   including those from the North China Plain (especially Shandong Provice) and the

Atmospheric
Chemistry
and Physics
Discussions

Open Access

310   neighboring provinces of Henan, Jiangsu, Jiangxi and Hubei. Long-range transport

311   could also impact the seasonal variations of atmospheric mercury in Hefei. As shown

312   in Figure 6, in spring, the major contributors of atmospheric mercury to Hefei were

313   from the southwestern region including the local area and the Jiangxi and Hunan

314   provinces. In summer, the main contributors were from north of Anhui, as well as

315   Henan and Jiangxi provinces, and even from the Pearl River Delta region in the far

316   south. In autumn and winter, the prevalent seasons for haze pollution, the most

317   important anthropogenic mercury sources to the monitoring site were the local

318   emissions and those from the neighboring region of Shandong, Henan and the Yangtze

319   River Delta region. The total mercury emissions from Henan and Shandong provinces

320   were estimated to be over 50 and 45 tons in 2010, respectively, making them two

321   largest Hg emitters in China (Zhang et al., 2015b).

322   GEM and CO normally share anthropogenic emission sources, such as industrial

323   and domestic coal combustion (Wu et al., 2006). However, they also have their own

324   sources, vehicles are another kind of dominant sources for CO, while power plants are

325   another type of mainly sources for GEM. The correlation between the concentrations

326   of GEM and CO during non-haze and haze days is shown in Fig. S2. The slope of the

327   trend line represents the Hg/CO ratio. Emissions from power plants typically have a

328   higher Hg/CO ratio (Wu et al., 2006), whereas biomass burning and residential coal

329   combustion have a lower Hg/CO ratio due to incomplete combustion (Weiss-Penzias

330   et al., 2007). The Hg/CO ratios from our study for both non-haze and haze days are in

331   the range of 0.0003-0.0009 ng m^{-3} ppbv^{-1}, similar to the ratio reported for Alaska

332   biomass burning (0.0014 ± 0.0006 ng m^{-3} ppbv^{-1}; Weiss-Penzias et al., 2007),

333   indicating that biomass burning might have played an important role in mercury

Atmospheric
Chemistry
and Physics
Discussions

334   emission in Hefei. This is further supported by the concentration of water-soluble

335   potassium (K^+) in PM_{10}. K^+ is a typical component of biomass burning aerosol and

336   has been used as a tracer element for qualitative identification of biomass burning

337   (Cachier et al., 1991). As shown in Fig. S3, K^+ in PM_{10} shows a good correlation with

338   air quality index (AQI) during the heavy pollution period of Nov-Dec, 2013. In

339   addition, seven high-GEM events were identified during the whole monitoring period

340   (Table S1). 5-day backward trajectories for each GEM heavy pollution event for the

341   time of at maximum GEM concentration are shown in Fig. S4. Air masses with

342   elevated GEM concentration were mainly from NW, SW and East directions. In

343   combination with the NASA's satellite hotspots/fire locations information from the

344   Fire Information for Resource Management System (FIRMS), there were potential

345   biomass burning occurred in these regions when air masses passed over (Fig. S4,

346   Events 1-7). Therefore, biomass burning can contribute to the observed higher mercury

347   concentrations, which not only came from local sources (Events 1 and 4), but could also

348   be affect by other regions through long-range transport processes (Events 2, 3, 6 and 7).

349

350   **4.2 Impacts of meteorological factors for atmospheric mercury during haze days**

351   Meteorological condition, especially wind direction and speed, could also impact

352   the atmospheric mercury during haze days. The wind rose for the monitoring site

353   during the study period is shown in Fig. 7. Easterly and southeasterly winds

354   represented the prevailing wind directions at the study site. A wind rose diagram of

355   GEM concentrations above the 90th percentile value is shown in Fig. 7B. We found

356   that 67% of the high GEM concentrations occurred at low wind speed (below 1.5 m

357   s^{-1}); however, wind speed below 1.5 m s^{-1} accounted for only 1.7% of total study.

Atmospheric
Chemistry
and Physics
Discussions

358   High RGM and PBM concentrations appear not to be related to high wind speed

359   (wind speed: 3-5 m s^{-1}); only 1.4% and 2.6% of the high RGM and PBM

360   concentrations were observed under high wind-speed conditions, respectively (Figs.

361   7C and 7D). In general, most of the high atmospheric mercury levels occurred in the

362   low wind speed conditions. This slow wind speed condition is not conductive to the

363   spread of mercury and thus favours the accumulation of atmospheric mercury,

364   especially during haze days.

365   Both GEM and PBM concentrations exhibited great variations with elevated

366   concentration during night or early morning, regardless of the presence of haze. Such a

367   diurnal variation of GEM and PBM could be related to changes in the height of urban

368   boundary layer, which is typically low in the morning and night, and high during the

369   daytime (Yuan et al., 2005;Mao et al., 2006). The maximum PBM concentration

370   (observed at 6:00) was more than 4 times higher than the minimum value (observed at

371   16:00) both under non-haze and haze days, and about 76% PBM were removed during

372   this period (6:00-16:00). However, the reductions of PBM as a result of deposition

373   during haze days was 62.7 pg m^{-3}, which was about 2.4 times that in non-haze days,

374   suggesting that haze pollution could increase the removal of PBM and thus reduce its

375   atmospheric lifetime. Although PBM is not the major form of mercury emitted to the

376   atmosphere, it is crucial in atmospheric mercury transport and removal processes due to

377   its short atmospheric lifetime. As shown in Fig. 8, the PBM concentration co-varied

378   with the $PM_{2.5}$ concentration, especially in January when all the four PBM peak events

379   were associated with increased $PM_{2.5}$ concentrations. The co-variation in February is

380   weaker, possibly due to the loss of PBM data because of instrument maintenance (see

381   Section 2.3). Elevated PBM concentrations might be due to the poor diffusion

Atmospheric
Chemistry
and Physics
Discussions

382 conditions in cold months and high PM pollution. Although the concentrations of $PM_{2.5}$

383 were similar from March to June, March showed higher PBM concentrations. This

384 might be due to higher temperatures in the warmer months which do not favor mercury

385 adsorption (Otani et al., 1986). These results indicate that both the $PM_{2.5}$ concentration

386 and temperature may play an important role in the formation of PBM.

387

388 **4.3 Chemical process for RGM and the potential oxidation mechanism**

389   In contrast with the diurnal variations of GEM and PBM, RGM shows different

390 diurnal trend. The RGM concentration during daytime was slightly higher than at

391 night. As discussed before in 4.2 section, the diurnal variation of GEM and PBM

392 could be related to changes in the height of urban boundary layer. So the role of

393 boundary layer for the enhancement of RGM during daytime would be limited. The

394 weak correlation (r=0.164, p<0.001) between RGM and CO suggests that regional

395 anthropogenic sources are not a major source of RGM in the air. As shown in Fig. 9

396 (haze days), the peak value of RGM coincided well with the lowest value of CO,

397 suggesting that the production of RGM in haze days does not fully come from

398 anthropogenic emission sources. Instead, RGM is more likely produced from the in

399 situ oxidation of GEM; this is supported by the fact that the peak values of RGM

400 coincided well with the decline of GEM. We found that the RGM concentration did

401 not change much from 8:00 to 20:00 (local time) during haze days. This indicates that

402 photochemical reaction between GEM and RGM still takes place during haze days,

403 but the daytime change in the intensity of solar radiation has been greatly dampened

404 due to the light-haze interaction.

405   Various atmospheric oxidants are capable of oxidizing GEM to RGM, including

406   halogen radicals, ozone, hydroxyl radicals (OH), among others (Holmes et al.,

407   2010;Wang et al., 2014). Halogen radicals, especially bromine atoms, are believed to

408   be the the primary oxidant for GEM in the global tropopshere (Holmes et al., 2010).

409   Unfortunately, we did not measure halogen radicals in this study. Ozone itself is not

410   an efficient oxidant for GEM oxidation due to low reaction rate (Hall, 1995;Holmes et

411   al., 2010). In the lower troposphere, ozone is produced from daytime photochemical

412   reactions involving volatile organic compounds (VOC) and nitrogen oxides (NO_x).

413   Due to fresh emissions of NO from vehicles can react with O_3 to form NO_2, so ozone

414   could not fully represent photochemical oxidation processes in urban area (Herndon et

415   al., 2008). Compared with ozone, odd oxygen ($O_X = O_3+NO_2$) is a more conserved

416   tracer of the extent of photochemical processing in the urban atmosphere (Herndon et

417   al., 2008;Wood et al., 2010). Because of such NO_2 concentrations from MAX-DOAS

418   are available only during the daytime, so we could only use O_X to be a indicator for

419   GEM oxidation occurred in the daytime. Diurnal variations of GEM, RGM and

420   Gas-Phase Data (O_X, O_3, NO_2 and CO) concentrations during non-haze and haze days

421   are shown in Fig. 9. The increase of O_X is consistent with the increase of RGM during

422   haze days, but seems to lag behind the increase of RGM during non-haze days,

423   suggesting some oxidation processes might be at work during haze days. During haze

424   days, both the RGM and O_X reached highest values around 16:00, along with the

425   lowest value of GEM, indicating the chemical transformation between GEM and

426   RGM occurred. However, this phenemenon is not found in non-haze days.

427   The OH radical is also an important oxidant for mercury in the atmosphere.

428   Previous studies have shown that the major source of OH in the early morning is the

Atmospheric
Chemistry
and Physics
Discussions

429   photolysis of HONO, which accumulates in the urban atmospheric boundary layer

430   during night (Kleffmann et al., 2005). The formation of HgOH as an intermediate

431   product of the Hg^0 (g) + OH oxidation reactions has been proposed by (Sommar et al.,

432   2001), although HgOH is highly unstable and could decompose back rapidly to Hg^0

433   and OH (Goodsite et al., 2004). It has been proposed that secondary reactants such as

434   NO_2, HO_2, RO, RO_2, and NO could assist the formation of Hg(II) from the initial

435   HgOH intermediate, which outcompetes with the decomposition of HgOH (Calvert

436   and Lindberg, 2005). As an example, we calculated the transformation between GEM

437   and RGM under the influence of NO_2, using the reactions and rate constants shown in

438   Table S2. As shown in Fig. S5, the production rate of NO_2HgOH, $d[NO_2HgOH]/dt$,

439   increased almost linearly with increasing NO_2 under low NO_2 concentrations, and

440   eventually reached a steady state when the NO_2 concentration is high enough.

441   Based on the production rate of NO_2HgOH, we can estimate the production of

442   NO_2HgOH during the 1 hr sampling period when RGM was captured by the

443   KCl-coated denuder in the Tekran 1130 unit. As discussed earlier, a distinct diurnal

444   relationship between GEM and RGM was observed both in non-haze and haze days

445   (Fig. 9). The production of NO_2HgOH and $d[NO_2HgOH]/dt$ corresponding to

446   different NO_2 concentrations is shown in Table 3. With the increase of the NO_2

447   concentration, the contribution of the NO_2HgOH production to RGM will increase. If

448   the NO_2 concentration is within 100 ppbv (from 0 to 100 ppbv), the production of

449   NO_2HgOH would be in range of 0.058-4.81 pg m^{-3} during the 1h sampling period.

450   The mean NO_2 concentration during haze days is 24.3 ppbv (unit converion see the

451   supporting information), which is higher that in non-haze days (17.4 ppbv). The

452   increments of RGM from sunrise to peak (6:00-12:00) are about 2.14 pg m^{-3} (growth

Atmospheric
Chemistry
and Physics
Discussions

453   rate ≈ 0.36 pg m^{-3} h^{-1}) and 0.41 pg m^{-3} (growth rate ≈ 0.068 pg m^{-3} h^{-1}) during haze

454   days and non-haze days, respectively. As illustrated in Table 3, the level of NO2 in the

455   urban atmosphere is enough for the production of RGM during the 1h sampling

456   period. In addition, we found that the NO$_2$ concentrations increased rapidly after

457   sunrise to reach peak values around noon, consistent with the increases of RGM

458   during haze days. We thus postulate that NO$_2$ aggregation with HgOH may be a

459   possible mechanism to explain the enhanced production of RGM during the daytime

460   over the inland urban air. The NO$_2$ level in urban air might have a more important

461   influence on the chemical transformations between the GEM and RGM during haze

462   days, rather than non-haze days. But unfortunately, we can not provide an adequate

463   description about these oxidation processes. To solve this problem, new laboratory

464   and mercury model studies on mercury oxidation mechanism are needed.

465

466   **5. Summary**

467   Continuous measurements of speciated atmospheric mercury were conducted at

468   Hefei, a mid-latitude inland city in central China, from July 2013 to June 2014.

469   Measurements of other trace gases (e.g. CO, O$_3$, NO$_2$) and meteorological parameters

470   were employed to better understand the sources and oxidation pathways of

471   atmospheric mercury. The mean GEM, RGM and PBM concentrations during haze

472   days were 4.74 ±1.62 ng m^{-3}, 4.32 ± 8.36 pg m^{-3} and 60.2 ± 131.4 pg m^{-3}, respectively.

473   Potential source contribution function (PSCF) analysis suggested that the local

474   mercury emission rather than long-range transport is the most important contributor of

475   atmospheric mercury pollution during haze days at our monitoring site. The Hg/CO

476   ratio and NASA's satellite fire locations information indicated that the biomass

Atmospheric
Chemistry
and Physics
Discussions

Open Access

EGU

477 burning may plays an important role in mercury emission. Haze pollution has

478 considerable impact on PBM rather than on GEM and RGM. Both GEM and PBM

479 concentrations exhibited greatly variations with elevated concentration during night.

480 The diurnal variations of GEM and PBM might be related to the boundary layer depth;

481 a lower boundary layer depth in the morning and night could elevate the mercury

482 concentration. The slow wind speed condition is not conductive to the spread of

483 mercury and thus favours the accumulation of atmospheric mercury, especially during

484 haze days. We found that PBM concentrations co-varied with the $PM_{2.5}$ concentration

485 especially in January when all the four PBM peak events were associated with

486 increased $PM_{2.5}$ concentrations. In addition, PBM showed a remarkable seasonal

487 pattern, with higher concentrations in cold seasons and lower in warm seasons.

488 Elevated PBM concentrations might be due to both the high loadings of particle

489 matter and disadvantageous diffusion conditions during haze days especially in cold

490 months. The peaks of RGM were observed around noon, which is probably due to the

491 higher intensity of solar radiation and photochemical oxidation processes at this time.

492 Change in the odd oxygen ($O_X = O_3 + NO_2$) concentration is normally appllied to be an

493 indicator for photochemical reaction. The increase of O_X is consistent with the

494 increase of RGM during haze days, but seems to lag behind the increase of RGM

495 during non-haze days, suggesting some oxidation processes might be at work during

496 haze days. Based on HgOH as an intermediate product, we suggest that NO_2

497 aggregation with HgOH is a potential mechanism to explain the enhanced production

498 of RGM during the daytime over the inland urban air. The NO_2 level in urban air

499 might have a more important influence on the chemical transformations between the

500 GEM and RGM during haze days, rather than non-haze days.

Atmospheric
Chemistry
and Physics
Discussions

Open Access

505

506

507   **References**

508   Brooks, S., Luke, W., Cohen, M., Kelly, P., Lefer, B., and Rappenglück, B.: Mercury

509   species measured atop the Moody Tower TRAMP site, Houston, Texas,

510   Atmospheric Environment, 44, 4045-4055, 2010.

511   Cachier, H., Ducret, J., Bremond, M., Yoboue, V., Lacaux, J., Gaudichet, A., and

512   Baudet, J.: Biomass burning aerosols in a savanna region of the Ivory Coast, in:

513   Global biomass burning. Atmospheric, climatic, and biospheric implications, 1991.

514   Calvert, J. G., and Lindberg, S. E.: Mechanisms of mercury removal by O_3 and OH in

515   the atmosphere, Atmospheric Environment, 39, 3355-3367, 2005.

516   Chen, L.-W. A., Chow, J. C., Doddridge, B. G., Dickerson, R. R., Ryan, W. F., and

517   Mueller, P. K.: Analysis of a summertime $PM_{2.5}$ and haze episode in the

518   mid-Atlantic region, Journal of the Air & Waste Management Association, 53,

519   946-956, 2003.

520   Cheng, I., Zhang, L., Mao, H., Blanchard, P., Tordon, R., and Dalziel, J.: Seasonal and

521   diurnal patterns of speciated atmospheric mercury at a coastal-rural and a

522   coastal-urban   site,   Atmospheric   Environment,   82,   193-205,

523   doi:10.1016/j.atmosenv.2013.10.016, 2014.

Atmospheric
Chemistry
and Physics
Discussions

524   Dommergue, A., Ferrari, C. P., Planchon, F. A., and Boutron, C. F.: Influence of

525   anthropogenic sources on total gaseous mercury variability in Grenoble suburban air

526   (France), Science of the total environment, 297, 203-213, 2002.

527   Draxler, R. R., and Hess, G.: An overview of the HYSPLIT_4 modelling system for

528   trajectories, Australian meteorological magazine, 47, 295-308, 1998.

529   Duan, L., Xiu, G., Feng, L., Cheng, N., and Wang, C.: The mercury species and their

530   association with carbonaceous compositions, bromine and iodine in $PM_{2.5}$ in

531   Shanghai, Chemosphere, 146, 263-271, 2016.

532   Fain, X., Obrist, D., Hallar, A., Mccubbin, I., and Rahn, T.: High levels of reactive

533   gaseous mercury observed at a high elevation research laboratory in the Rocky

534   Mountains, Atmospheric Chemistry and Physics, 9, 8049-8060, 2009.

535   Fang, F., Wang, Q., and Li, J.: Atmospheric particulate mercury concentration and its

536   dry deposition flux in Changchun City, China, Science of the total environment, 281,

537   229-236, 2001.

538   Fang, F., Wang, Q., and Li, J.: Urban environmental mercury in Changchun, a

539   metropolitan city in Northeastern China: source, cycle, and fate, Science of the Total

540   Environment, 330, 159-170, 2004.

541   Fang, G.-C., Wu, Y.-S., and Chang, T.-H.: Comparison of atmospheric mercury (Hg)

542   among Korea, Japan, China and Taiwan during 2000–2008, Journal of hazardous

543   materials, 162, 607-615, 2009.

544   Feng, X., Shang, L., Wang, S., Tang, S., and Zheng, W.: Temporal variation of total

545   gaseous mercury in the air of Guiyang, China, Journal of Geophysical Research:

546   Atmospheres (1984–2012), 109, 2004.

Atmospheric
Chemistry
and Physics
Discussions

Open Access

EGU

547   Friedli, H., Arellano Jr, A., Geng, F., Cai, C., and Pan, L.: Measurements of

548   atmospheric mercury in Shanghai during September 2009, Atmospheric Chemistry

549   and Physics, 11, 3781-3788, 2011.

550   Fu, X., Feng, X., Zhu, W., Wang, S., and Lu, J.: Total gaseous mercury concentrations

551   in ambient air in the eastern slope of Mt. Gongga, South-Eastern fringe of the

552   Tibetan plateau, China, Atmospheric Environment, 42, 970-979, 2008a.

553   Fu, X., Feng, X., Zhu, W., Zheng, W., Wang, S., and Lu, J. Y.: Total particulate and

554   reactive gaseous mercury in ambient air on the eastern slope of the Mt. Gongga area,

555   China, Applied Geochemistry, 23, 408-418, 2008b.

556   Fu, X., Feng, X., Qiu, G., Shang, L., and Zhang, H.: Speciated atmospheric mercury

557   and its potential source in Guiyang, China, Atmospheric Environment, 45,

558   4205-4212, 2011.

559   Fu, X., Feng, X., Liang, P., Zhang, H., Ji, J., and Liu, P.: Temporal trend and sources of

560   speciated atmospheric mercury at Waliguan GAW station, Northwestern China,

561   Atmospheric Chemistry and Physics, 12, 1951-1964, 2012.

562   Goodsite, M. E., Plane, J., and Skov, H.: A theoretical study of the oxidation of Hg^0 to

563       $HgBr_2$ in the troposphere, Environmental science & technology, 38, 1772-1776,

564   2004.

565   Gustin, M., and Jaffe, D.: Reducing the uncertainty in measurement and understanding

566   of mercury in the atmosphere, Environmental science & technology, 44, 2222-2227,

567   2010.

568   Gustin, M., Amos, H., Huang, J., Miller, M., and Heidecorn, K.: Measuring and

569   modeling mercury in the atmosphere: a critical review, Atmospheric Chemistry and

570   Physics, 15, 5697-5713, 2015.

Atmospheric
Chemistry
and Physics
Discussions

Open Access

571   Gustin, M. S., Huang, J., Miller, M. B., Peterson, C., Jaffe, D. A., Ambrose, J., Finley, B.

572   D., Lyman, S. N., Call, K., and Talbot, R.: Do we understand what the mercury

573   speciation instruments are actually measuring? Results of RAMIX, Environmental

574   science & technology, 47, 7295-7306, 2013.

575   Hall, B.: The gas phase oxidation of elemental mercury by ozone, in: Mercury as a

576   Global Pollutant, Springer, 301-315, 1995.

577   Herndon, S. C., Onasch, T. B., Wood, E. C., Kroll, J. H., Canagaratna, M. R., Jayne, J.

578   T., Zavala, M. A., Knighton, W. B., Mazzoleni, C., and Dubey, M. K.: Correlation of

579   secondary organic aerosol with odd oxygen in Mexico City, Geophysical Research

580   Letters, 35, 2008.

581   Holmes, C. D., Jacob, D. J., Corbitt, E. S., Mao, J., Yang, X., Talbot, R., and Slemr, F.:

582   Global atmospheric model for mercury including oxidation by bromine atoms,

583   Atmospheric Chemistry and Physics, 10, 12037-12057, 2010.

584   Hu, Q.-H., Kang, H., Li, Z., Wangv, Y.-S., Ye, P.-P., Zhang, L.-L., Yu, J., Yu, X.-W., Sun,

585   C., and Xie, Z.-Q.: Characterization of atmospheric mercury at a suburban site of

586   central China from wintertime to springtime, Atmospheric Pollution Research, 5,

587   2014.

588   Huang, J., Miller, M. B., Weiss-Penzias, P., and Gustin, M. S.: Comparison of gaseous

589   oxidized Hg measured by KCl-coated denuders, and nylon and cation exchange

590   membranes, Environmental science & technology, 47, 7307-7316, 2013.

591   Kleffmann, J., Gavriloaiei, T., Hofzumahaus, A., Holland, F., Koppmann, R., Rupp, L.,

592   Schlosser, E., Siese, M., and Wahner, A.: Daytime formation of nitrous acid: A

593   major source of OH radicals in a forest, Geophysical Research Letters, 32, 2005.

Atmospheric
Chemistry
and Physics
Discussions

594   Landis, M. S., Stevens, R. K., Schaedlich, F., and Prestbo, E. M.: Development and

595   characterization of an annular denuder methodology for the measurement of

596   divalent inorganic reactive gaseous mercury in ambient air, Environmental science

597   & technology, 36, 3000-3009, 2002.

598   Li, J., Sommar, J., Wängberg, I., Lindqvist, O., and Wei, S.-q.: Short-time variation of

599   mercury speciation in the urban of Göteborg during GÖTE-2005, Atmospheric

600   Environment, 42, 8382-8388, 2008.

601   Lindberg, S., Bullock, R., Ebinghaus, R., Engstrom, D., Feng, X., Fitzgerald, W.,

602   Pirrone, N., Prestbo, E., and Seigneur, C.: A synthesis of progress and uncertainties

603   in attributing the sources of mercury in deposition, AMBIO: A Journal of the

604   Human Environment, 36, 19-33, 2007.

605   Lindberg, S. a., and Stratton, W.: Atmospheric mercury speciation: concentrations and

606   behavior of reactive gaseous mercury in ambient air, Environmental Science &

607   Technology, 32, 49-57, 1998.

608   Lindqvist, O., and Rodhe, H.: Atmospheric mercury-a review*, Tellus B, 37, 1985.

609   Liu, B., Keeler, G. J., Dvonch, J. T., Barres, J. A., Lynam, M. M., Marsik, F. J., and

610   Morgan, J. T.: Urban–rural differences in atmospheric mercury speciation,

611   Atmospheric Environment, 44, 2013-2023, 2010.

612   Ma, J., Beirle, S., Jin, J., Shaiganfar, R., Yan, P., and Wagner, T.: Tropospheric NO_2

613   vertical column densities over Beijing: results of the first three years of

614   ground-based MAX-DOAS measurements (2008–2011) and satellite validation,

615   Atmospheric Chemistry and Physics, 13, 1547-1567, 2013.

Atmospheric
Chemistry
and Physics
Discussions

Open Access

EGU

616   Mao, M., Jiang, W., Wu, X., Qi, F., Yuan, R., Fang, H., Liu, D., and Zhou, J.: LIDAR

617   exploring of the UBL in downtown of the Nanjing City, Acta Scientiae

618   Circumstantiae, 26, 1723-1728, 2006.

619   Otani, Y., Kanaoka, C., Usui, C., Matsui, S., and Emi, H.: Adsorption of mercury vapor

620   on particles, Environmental science & technology, 20, 735-738, 1986.

621   Pacyna, E. G., Pacyna, J. M., Steenhuisen, F., and Wilson, S.: Global anthropogenic

622   mercury emission inventory for 2000, Atmospheric environment, 40, 4048-4063,

623   2006.

624   Polissar, A. V., Hopke, P. K., and Harris, J. M.: Source regions for atmospheric aerosol

625   measured at Barrow, Alaska, Environmental science & technology, 35, 4214-4226,

626   2001.

627   Schroeder, W. H., and Munthe, J.: Atmospheric mercury-an overview, Atmospheric

628   Environment, 32, 809-822, 1998.

629   Sommar, J., Gårdfeldt, K., Strömberg, D., and Feng, X.: A kinetic study of the

630   gas-phase reaction between the hydroxyl radical and atomic mercury, Atmospheric

631   Environment, 35, 3049-3054, 2001.

632   Stamenkovic, J., Lyman, S., and Gustin, M. S.: Seasonal and diel variation of

633   atmospheric mercury concentrations in the Reno (Nevada, USA) airshed,

634   Atmospheric Environment, 41, 6662-6672, 2007.

635   Streets, D. G., Hao, J., Wu, Y., Jiang, J., Chan, M., Tian, H., and Feng, X.:

636   Anthropogenic mercury emissions in China, Atmospheric Environment, 39,

637   7789-7806, 2005.

Atmospheric
Chemistry
and Physics

Discussions

Open Access

EGU

638   Sun, Z., Mu, Y., Liu, Y., and Shao, L.: A comparison study on airborne particles during

639   haze days and non-haze days in Beijing, Science of the total environment, 456, 1-8,

640   2013.

641   Wan, Q., Feng, X., Lu, J., Zheng, W., Song, X., Han, S., and Xu, H.: Atmospheric

642   mercury in Changbai Mountain area, northeastern China I. The seasonal distribution

643   pattern of total gaseous mercury and its potential sources, Environmental research,

644   109, 201-206, 2009a.

645   Wan, Q., Feng, X., Lu, J., Zheng, W., Song, X., Li, P., Han, S., and Xu, H.: Atmospheric

646   mercury in Changbai Mountain area, northeastern China II. The distribution of

647   reactive gaseous mercury and particulate mercury and mercury deposition fluxes,

648   Environmental research, 109, 721-727, 2009b.

649   Wang, F., Saiz-Lopez, A., Mahajan, A., Mart ń, J. G., Armstrong, D., Lemes, M., Hay,

650   T., and Prados-Roman, C.: Enhanced production of oxidised mercury over the

651   tropical Pacific Ocean: a key missing oxidation pathway, Atmospheric Chemistry

652   and Physics, 14, 1323, 2014.

653   Wang, Y., Zhang, X., and Draxler, R. R.: TrajStat: GIS-based software that uses various

654   trajectory statistical analysis methods to identify potential sources from long-term

655   air pollution measurement data, Environmental Modelling & Software, 24, 938-939,

656   2009.

657   Weiss-Penzias, P., Jaffe, D., Swartzendruber, P., Hafner, W., Chand, D., and Prestbo, E.:

658   Quantifying Asian and biomass burning sources of mercury using the Hg/CO ratio

659   in pollution plumes observed at the Mount Bachelor Observatory, Atmospheric

660   Environment, 41, 4366-4379, 2007.

661 Wood, E., Canagaratna, M., Herndon, S., Onasch, T., Kolb, C., Worsnop, D., Kroll, J.,

662 Knighton, W., Seila, R., and Zavala, M.: Investigation of the correlation between

663 odd oxygen and secondary organic aerosol in Mexico City and Houston,

664 Atmospheric Chemistry and Physics, 10, 8947-8968, 2010.

665 Wu, Y., Wang, S., Streets, D. G., Hao, J., Chan, M., and Jiang, J.: Trends in

666 anthropogenic mercury emissions in China from 1995 to 2003, Environmental

667 science & technology, 40, 5312-5318, 2006.

668 Xu, X., and Akhtar, U.: Identification of potential regional sources of atmospheric total

669 gaseous mercury in Windsor, Ontario, Canada using hybrid receptor modeling,

670 Atmospheric Chemistry and Physics, 10, 7073-7083, 2010.

671 Yuan, S., Xin, Y., and Zhou, J.: Lidar Observations of the Lower Atmosphere in Hefei,

672 Chinese Journal of Atmospheric Sciences, 29, 387-395, 2005.

673 Zhang, H., Fu, X., Lin, C., Wang, X., and Feng, X.: Observation and analysis of

674 speciated atmospheric mercury in Shangri-La, Tibetan Plateau, China, Atmospheric

675 Chemistry and Physics, 15, 653-665, 2015a.

676 Zhang, L., Wang, S., Wang, L., and Hao, J.: Atmospheric mercury concentration and

677 chemical speciation at a rural site in Beijing, China: implications of mercury

678 emission sources, Atmospheric Chemistry and Physics, 13, 10505-10516, 2013.

679 Zhang, L., Wang, S., Wang, L., Wu, Y., Duan, L., Wu, Q., Wang, F., Yang, M., Yang, H.,

680 and Hao, J.: Updated Emission Inventories for Speciated Atmospheric Mercury

681 from Anthropogenic Sources in China, Environmental science & technology, 49,

682 3185-3194, 2015b.

683

Atmospheric
Chemistry
and Physics
Discussions

Open Access

EGU

684   **Table 1. Summary of GEM, RGM and PBM concentrations measured in Hefei**

685   **from July 2013 to June 2014.**

686

	GEM (ng m^{-3})			RGM (pg m^{-3})			PBM (pg m^{-3})		
	Mean$\pm\sigma$	Range	N	Mean$\pm\sigma$	Range	N	Mean$\pm\sigma$	Range	N
Spring	3.89$\pm$1.79	0.2-21.3	7890	4.49$\pm$4.22	0.5-69.8	526	8.34$\pm$8.97	1.6-130.1	542
Summer	4.08$\pm$1.99	0.3-22.9	6050	3.66$\pm$4.39	0.5-45.2	511	3.61$\pm$4.38	0.5-41.9	570
Autumn	4.51$\pm$2.10	0.4-23.8	3632	5.65$\pm$8.93	0.5-78.9	274	59.9$\pm$153.5	0.5-1615	339
Winter	4.05$\pm$1.81	0.9-12.2	6381	2.59$\pm$2.58	0.5-9.5	541	56.1$\pm$134.9	0.5-1827	639
Total	4.07$\pm$1.91	0.2-23.8	23953	3.67$\pm$5.11	0.5-78.9	1852	30.02$\pm$100.3	0.5-1827	2090
Non-haze	3.95$\pm$1.93	0.2-23.8	20345	2.49$\pm$2.41	0.5-33.5	1508	23.3$\pm$90.76	0.5-1827	1708
Haze	4.74$\pm$1.62	2.1-16.5	3608	4.32$\pm$8.36	0.5-78.9	344	60.2$\pm$131.4	1.6-1615	382

687

688

Atmospheric
Chemistry
and Physics
Discussions

689   **Table 2. Speciated atmospheric mercury concentrations in Hefei and other urban**

690   **and rural areas.**

691

692

Location	Classification	Time	TGM (ng m^{-3})	GEM (ng m^{-3})	RGM (pg m^{-3})	PBM (pg m^{-3})	Reference
Hefei	Suburb	Jul 2013-Jun 2014	4.1	4.07	3.67	30	This study
Hefei	Suburb	Feb-May 2009	2.53	-	-	-	Hu et al. (2014)
Beijing	Rural	Dec 2008-Nov 2009	3.23	3.22	10.1	98.2	Zhang et al. (2013)
Shanghai	Urban	Aug-Sep 2009	2.7	-	-	-	Friedli et al. (2011)
Nanjing	Urban	Jan-Dec 2011	7.9	-	-	-	Zhu et al. (2012)
Guiyang	Urban	Nov 2001-Nov 2002	8.4	-	-	-	Feng et al. (2004)
Guiyang	Urban	Aug-Dec 2009	-	9.72	35.7	368	Fu et al. (2011)
Changchun	Urban	Jul 1999-Jan 2000	18.4	-	-	276	Fang et al. (2004)
Changchun	Suburb	Jul 1999-Jan 2000	11.7	-	-	109	Fang et al. (2004)
Mt.Changbai	Remote	Aug 2005-Jul 2006	3.58	-	65	77	Wan et al. (2009a, b)
Mt.Gongga	Remote	May 2005-July 2006	3.98	-	6.2	30.7	Fu et al. (2008a, b)
Mt.Waliguan	Remote	Sep 2007-Aug 2008	1.98	-	7.4	19.4	Fu et al. (2012a)
Mt.Leigong	Remote	May 2008-May 2009	2.8	-	-	-	Fu et al. (2010)
Shangri-La	Remote	Nov 2009-Nov 2010	2.55	-	8.22	38.82	Zhang (2015)
Detroit, USA	Urban	Jan-Dec 2004	-	2.5	15.5	18.1	Liu et al. (2010)
Dexter, USA	Rural	Jan-Dec 2004	-	1.6	3.8	6.1	Liu et al. (2010)
Houston, USA	Urban	Aug-Oct 2006	-	1.66	6.9	2.5	Brooks et al. (2010)
Göteborg, Sweden	Urban	Feb-Mar 2005	-	1.96	2.53	12.5	Li et al. (2008)
Nova Scotia, Canada	Urban	Jan 2010- Dec 2011		1.67	2.07	2.32	Cheng et al. (2014)
Northern Hemisphere background value				1.5-1.7			Lindberg et al. (2007)

Atmospheric
Chemistry
and Physics
Discussions

693   **Table 3. The production of NO$_2$HgOH and d[NO$_2$HgOH]/dt at different NO$_2$**

694   **concentrations**

NO2 (ppbv)	10	20	30	40	50	60	70	80	90	100
d(NO$_2$HgOH)/dt (molecule cm^{-3} s^{-1})	0.36	0.71	1.04	1.37	1.68	1.99	2.28	2.56	2.83	3.10
NO2HgOH (pg m^{-3}, 1hr)	0.56	1.10	1.63	2.13	2.61	3.08	3.54	3.97	4.40	4.81

695

696

697

698
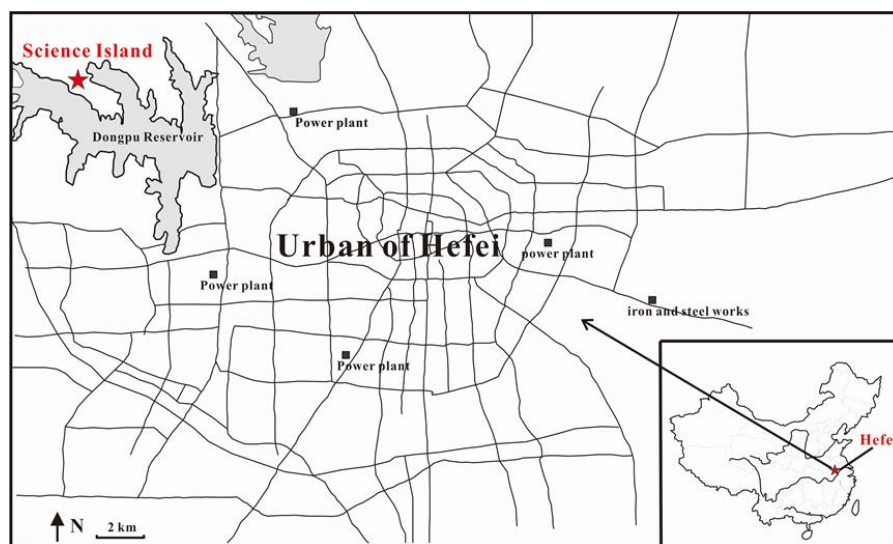
699   **Fig. 1.** Location of the monitoring site in Hefei, China.

700

Atmospheric
Chemistry
and Physics
Discussions
Open Access
EGU

701
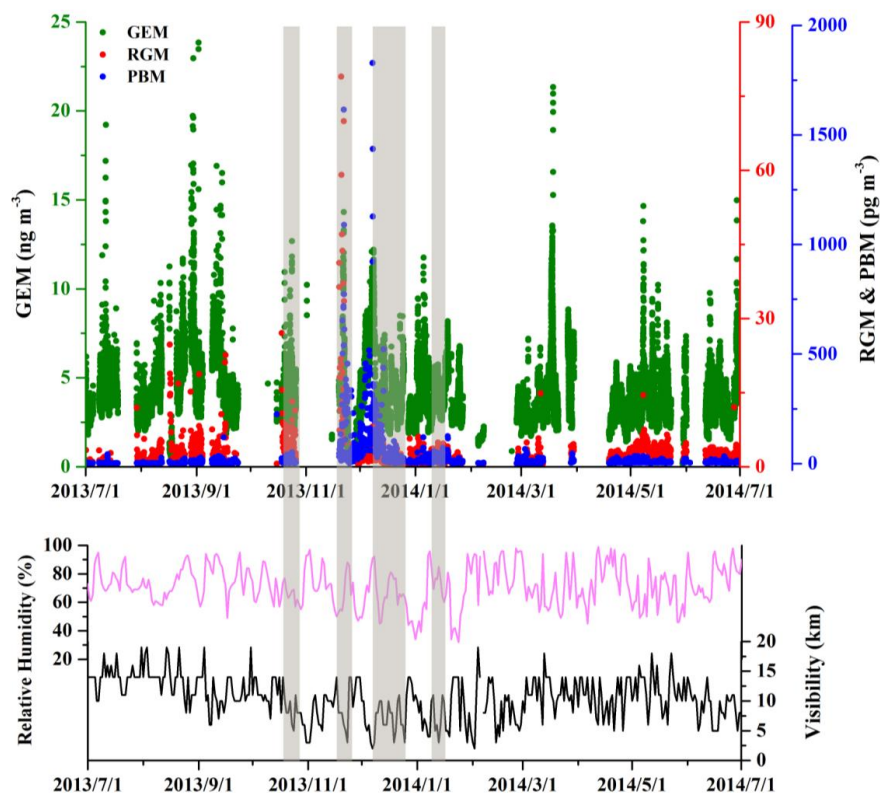
Fig. 2. Time series of GEM, RGM and PBM concentrations, along with visibility,

relatively humidity, at the monitoring site in Hefei from July 2013 to June 2014. The

GEM data were at a 5-min resolution, and the RGM and PBM data were two-hour

averages. The gray columns show the major haze pollution episodes occurred during

the study period.

707

Atmospheric
Chemistry
and Physics
Discussions
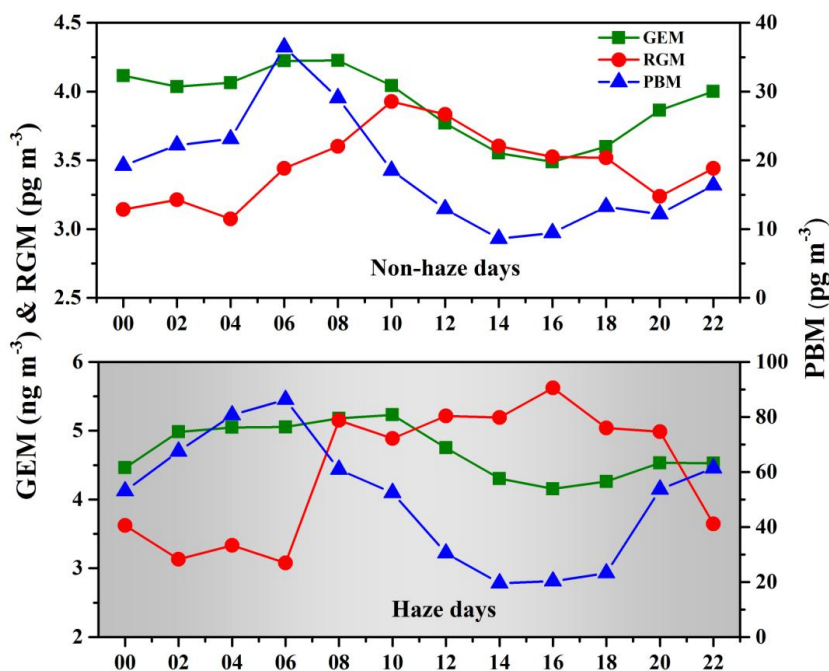
708

709   **Fig. 3.** Diurnal trends of GEM, RGM and PBM concentrations in Hefei during

710   non-haze and haze days (Local time = UTC + 8 hr). The data were two-hour averages.

711

Atmospheric
Chemistry
and Physics
Discussions

712
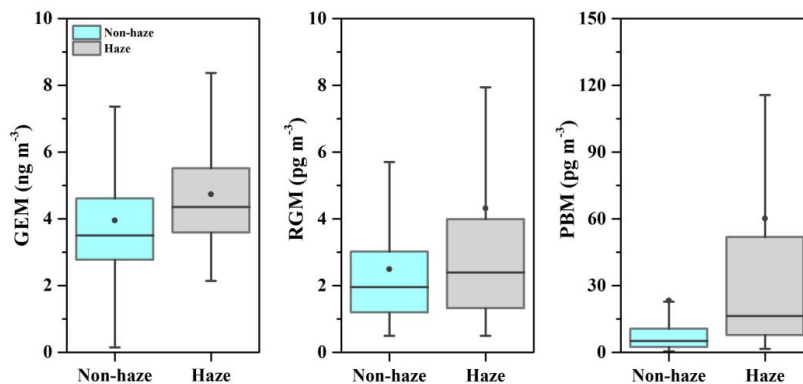
Fig. 4. GEM, RGM and PBM concentrations during non-haze and haze days. The

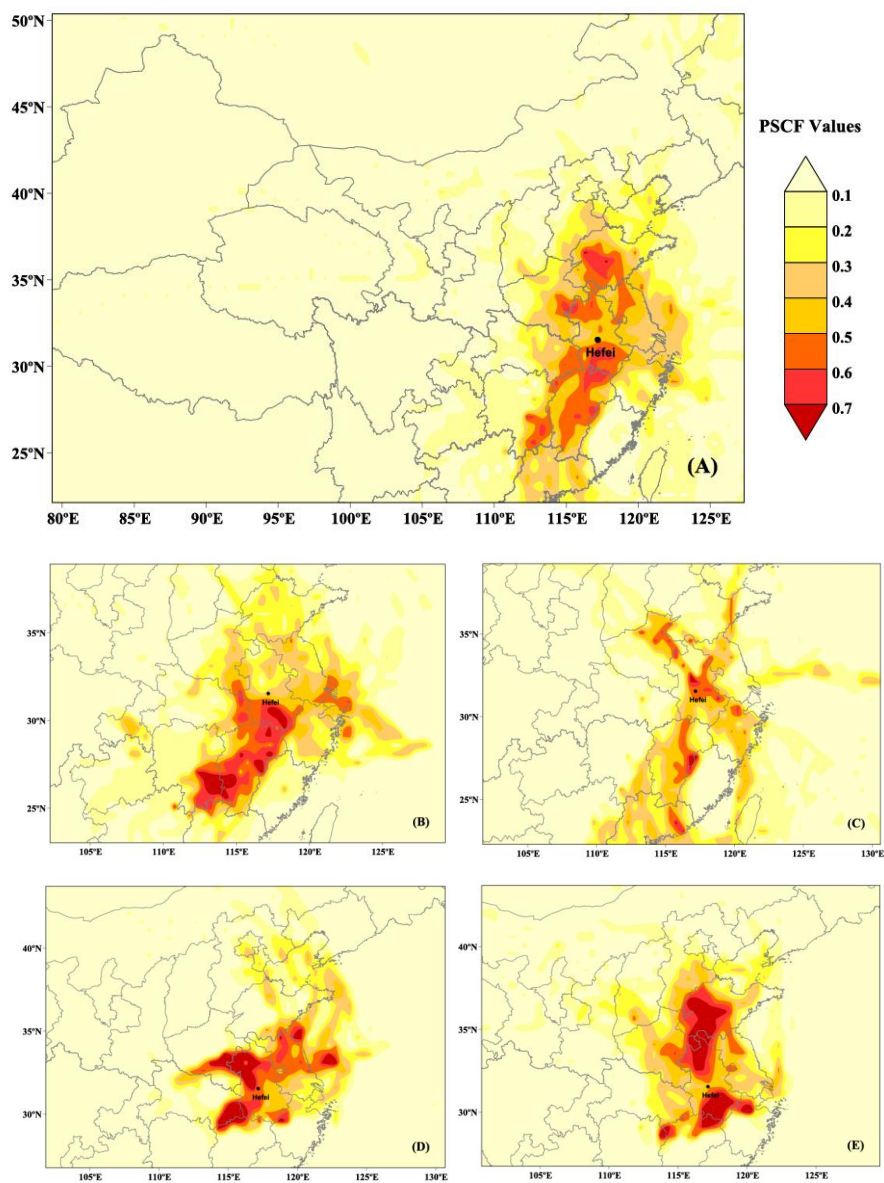GEM data were at a 5-min resolution, the RGM and PBM data were two-hour

averages.

716

Atmospheric
Chemistry
and Physics
Discussions

Open Access

EGU
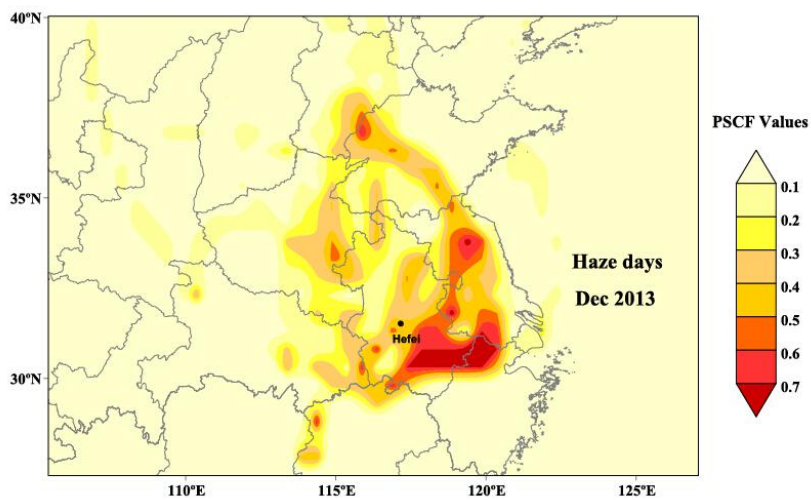
717
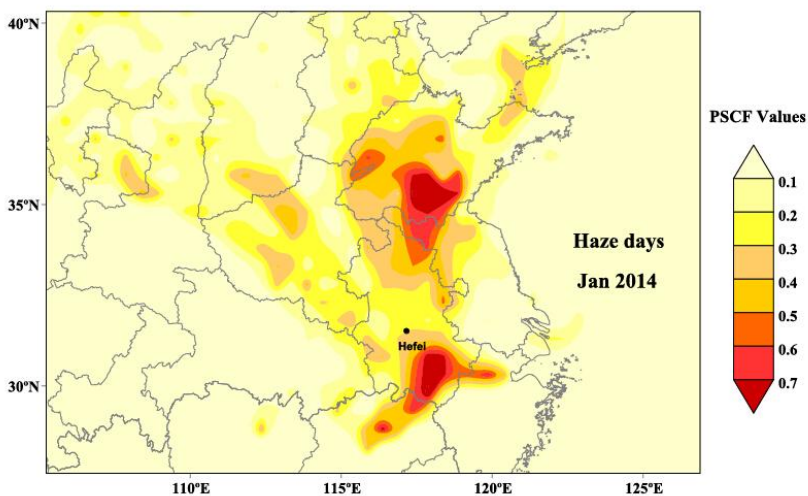
718

719   **Fig. 5.** Likely sources areas of GEM during haze days identified by PSCF analysis.

720

721
722
723
724
725
726
727
728
729
730
731
732

Fig. 6. Likely emission sources areas of GEM simulated by PSCF analysis. (A)

overall (from July 2013 to June 2014), (B) spring, (C) summer, (D) autumn, (E)

winter.

736

Atmospheric
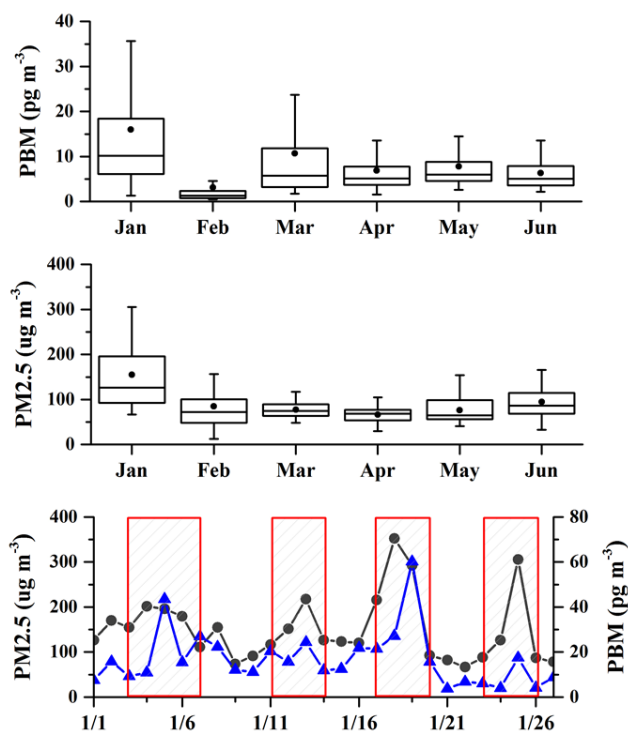Chemistry
and Physics
Discussions

Open Access
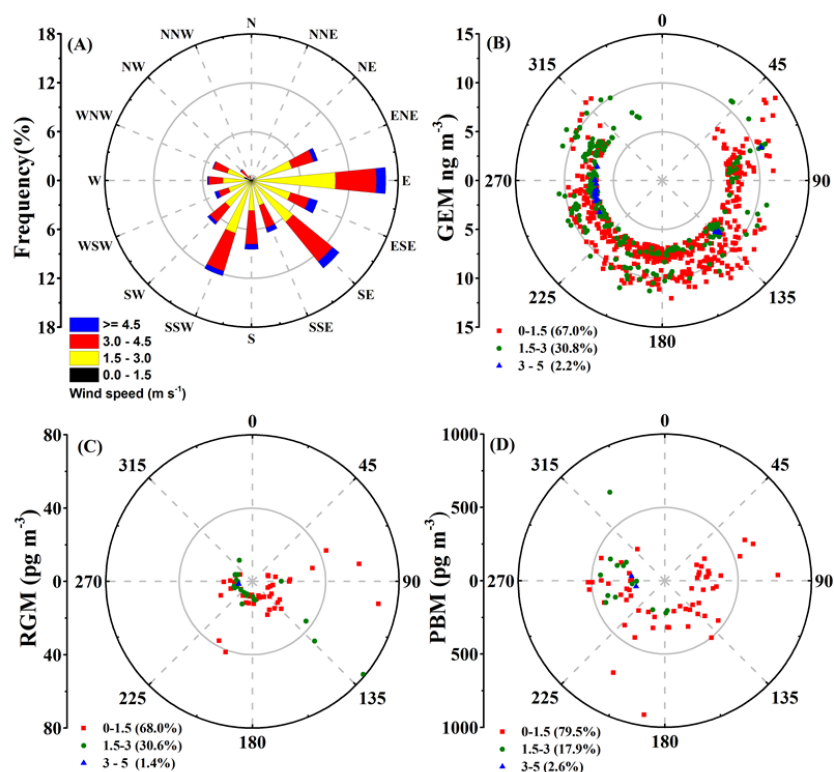
737

738

739   **Fig. 7.** Wind direction and speed at the Science Island Meteorological Station during

740   the study period. (A) the wind rose for the whole study period; (B), (C) and (D) are

741   the wind rose diagrams for GEM, RGM and PBM concentrations above the 90th

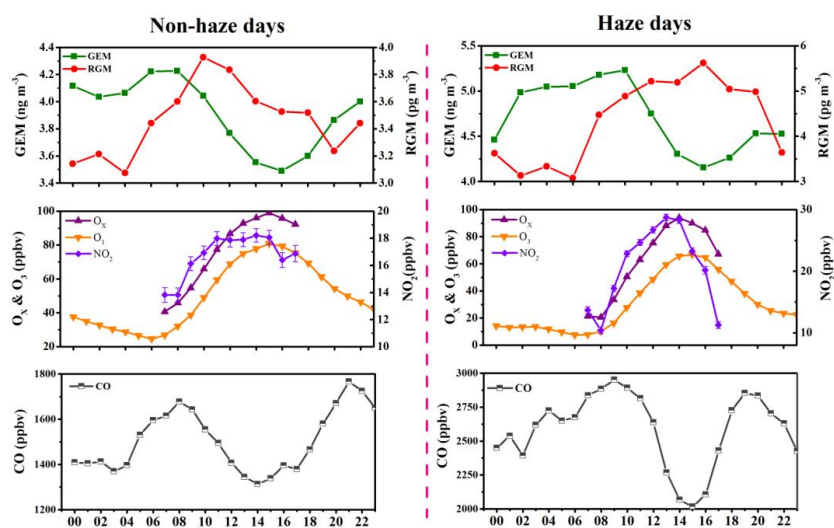742   percentile values, respectively.

743

744

745

Fig. 8. PBM and PM$_{2.5}$ concentrations from January to June, 2014.

747

748

Fig. 9. Diurnal variations of GEM, RGM and Gas-Phase Data (O_X, O_3, NO_2 and CO)

concentrations during non-haze and haze days. Notes: bottom is the carbon monoxide

mixing ratio. Middle are the averaged O_3, O_X ($O_X = NO_2 + O_3$) and NO_2 concentrations.

Top are the hourly averaged GEM and RGM concentrations. The bars for NO_2 refer to

the standard deviations.

754